Importance of Cold Pools to NCEP Mesoscale Eta Model Forecasts

DAVID J. STENSRUD

NOAA/ERL/National Severe Storms Laboratory, Norman, Oklahoma

GEOFFREY S. MANIKIN,* ERIC ROGERS, AND KENNETH E. MITCHELL

Environmental Modeling Center/National Centers for Environmental Prediction, Camp Springs, Maryland

(Manuscript received 24 September 1998, in final form 25 March 1999)

ABSTRACT

The cold pool, a pool of evaporatively cooled downdraft air that spreads out horizontally along the ground beneath a precipitating cloud, is often a factor in severe weather and heavy precipitation events. Unfortunately, cold pools are not well sampled by the present observational network and are rarely depicted in numerical model initial conditions. A procedure to identify and insert cold pools into the 29-km Eta Model is developed and tested on seven cases during 1995. Results suggest that when the large-scale forcing is strong, the inclusion of cold pools produces only slight changes in the forecasts. However, for the one case in which the large-scale forcing is relatively weak, the inclusion of cold pools produces significant changes in many of the model fields. These initial results, while not conclusive, suggest that the incorporation of cold pools, and other mesoscale features, may be important to the improvement of numerical guidance for severe weather and heavy precipitation forecasting.

1. Introduction

Severe weather and heavy precipitation forecasting are two of the most difficult aspects of operational forecasting (Charba and Klein 1980; Johns and Doswell 1992). Both rely heavily on parameter evaluation, pattern recognition, and a knowledge of the climatology of these events to produce the best possible forecasts (Funk 1991; Johns and Doswell 1992). During the past decade, numerical weather prediction models have played an increasingly important role in providing guidance to forecasters on the evolution of the parameters used to evaluate the potential for heavy precipitation and severe thunderstorms. However, as our understanding of these types of events has improved, the important roles played by mesoscale features have been highlighted (Maddox et al. 1979, 1980; Olson 1985; Doswell 1987; Funk 1991; Doswell et al. 1993). During the warm season, Heideman and Fritsch (1988) show that over 80% of the more significant precipitation events[1] are directly or indirectly related to thunderstorm activity. They conclude that increases in quantitative precipitation forecast (QPF) skill will be limited until operational models can predict mesoscale convective systems (MCSs) as well as they predict extratropical cyclones. Similarly, Johns and Doswell (1992) conclude that improvements in severe weather forecasting will depend in part on the ability of numerical models to accurately forecast changes in the critical severe weather parameters, which often have mesoscale structure. These studies strongly suggest that accurately including mesoscale features in numerical models is an important concern, yet evidence presented by Stensrud and Fritsch (1994a,b) and Gallus and Bresch (1997) suggests that one of the challenges to predicting these features is producing a realistic model initial condition that accurately captures the mesoscale environment at the model initial time.

One mesoscale feature that is known to influence convective evolution is the cold pool, a pool of evaporatively cooled downdraft air that spreads out horizontally along the ground beneath a precipitating cloud. Cold pools are important because some of the environmental

* Additional affiliation: SAIC/General Sciences Corporation, Laurel, Maryland.

Corresponding author address: Dr. David J. Stensrud, National Severe Storms Laboratory, 1313 Halley Circle, Norman, OK 73069. E-mail: David.Stensrud@nssl.noaa.gov

[1] They limited their analysis only to events in which rainfall of greater than 12.7 mm occurred over the contiguous United States east of 109°W during a 24-h period ending 1200 UTC.

© 1999 American Meteorological Society

Unauthenticated | Downloaded 05/11/21 01:50 AM UTC

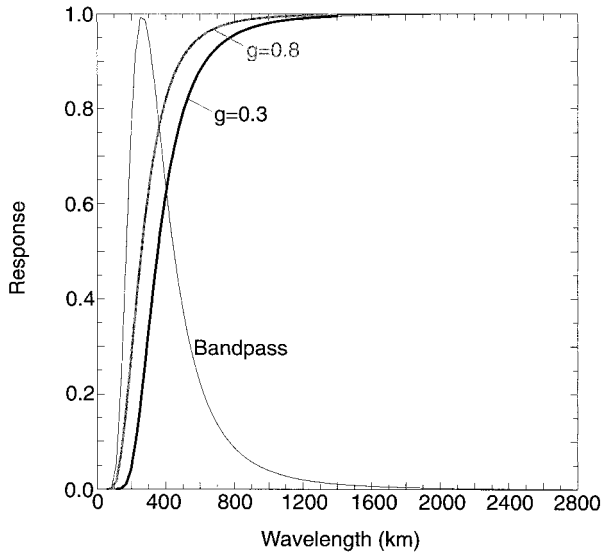

FIG. 1. Response curves vs wavelength (km) for objective analyses used in the cold pool identification procedure. Curves $g = 0.3$ (thick black line) and $g = 0.8$ (thick gray line) are the large and mesoscale analyses, respectively, used to define the mesoscale bandpass filter (thin solid line).

air approaching the cold pool likely will be lifted up and over it, and this lifting process is important to the development of new convection (Byers and Braham 1949; Wilson and Schreiber 1986). Case studies of the influences of mesoscale-sized cold pools (100–400 km in horizontal extent) on numerical weather prediction by Olson (1985), Stensrud and Fritsch (1994a,b), and Spencer and Stensrud (1998) illustrate clearly that cold pools are not captured easily in model initialization schemes owing to the lack of upper-air data with sufficient horizontal and temporal density. Without an appropriate vertical structure to support the surface observations within the cold pool, models quickly remove the spurious low-level pressure and temperature perturbations. The lack of this appropriate vertical structure may lead to the inaccurate development of convection within the cold pool region in numerical models, with detrimental effects on numerically generated QPFs and model guidance for severe weather forecasting.

For heavy precipitation forecasts, operational forecasting techniques have been developed to overcome some aspects of these model deficiencies by shifting the region of heaviest rainfall upstream of the cold pool with respect to the low-level flow (Funk 1991). These techniques consistently improve upon the numerical output (Mostek and Junker 1989; Funk 1991), although the month-to-month QPF skill scores indicate a close correspondence between the skill of the model and the skill of the human forecaster. Cold pools also are important contributors to flash flood events as documented by Maddox et al. (1979). These studies make it clear that improved numerical guidance, including information on cold pool strength and position, would be of benefit to operational heavy precipitation forecasting.

Cold pools also are important to the development and evolution of severe weather events. Thunderstorms are often seen to intensify as they cross a thermal boundary, such as a cold pool (Maddox et al. 1980). Cortinas and Stensrud (1995) illustrate that cold pools, as created by a numerical model, alter the environmental parameters, such as convective available potential energy (CAPE) and storm-relative environmental helicity (SREH) (Davies-Jones et al. 1990), that are used to help forecast supercell thunderstorms (Johns and Doswell 1992). While the exact mechanisms by which cold pools intensify thunderstorms are unknown, more accurate knowledge of the extent, intensity, and movement of cold pools would be useful for forecasting severe weather.

This manuscript reports on an exploratory effort to automatically define and insert mesoscale cold pool

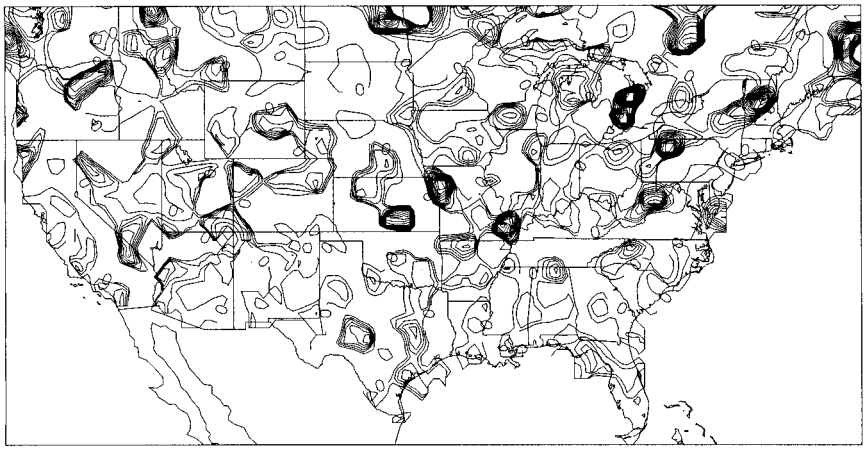

FIG. 2. Perturbation sea level pressure field (hPa) determined from the cold pool identification procedure at 1200 UTC 17 May 1995, where only positive values of the perturbation sea level pressure are contoured. Contour interval is 0.25 hPa.

Unauthenticated | Downloaded 05/11/21 01:50 AM UTC

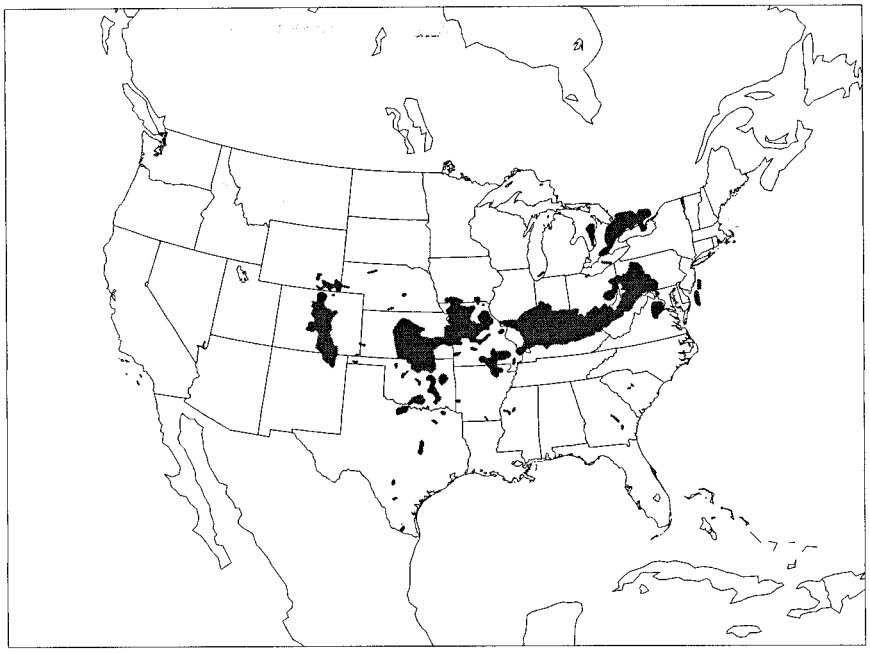

FIG. 3. National multisensor precipitation analysis for 1200 UTC 17 May 1995 where the shaded regions denote areas where precipitation is occurring over the 48 contiguous United States. Although the multisensor analysis includes estimates of the amounts of precipitation, the cold pool identification procedure does not use this information.

structures into the initial conditions for an operational numerical weather prediction model. Cold pools with horizontal scales of less than 100 km are not considered, since these cold pools cannot be resolved well by either the observations or the model. The numerical model chosen for use is described in section 2. Our procedure for identifying cold pools and inserting them into the model initial conditions is described in sections 3 and 4. Results are discussed in section 5, followed by a concluding discussion in section 6.

2. Model description

The model chosen for use in this study is the 29-km version of the three-dimensional hydrostatic Eta Model (Mesinger et al. 1988; Black 1994; Janjic 1994), which was run operationally at the National Centers for Environmental Prediction (NCEP) from August 1995 until 3 June 1998. During the time period over which this particular domain and grid spacing was used, this model configuration was referred to as the Mesoscale Eta Mod-

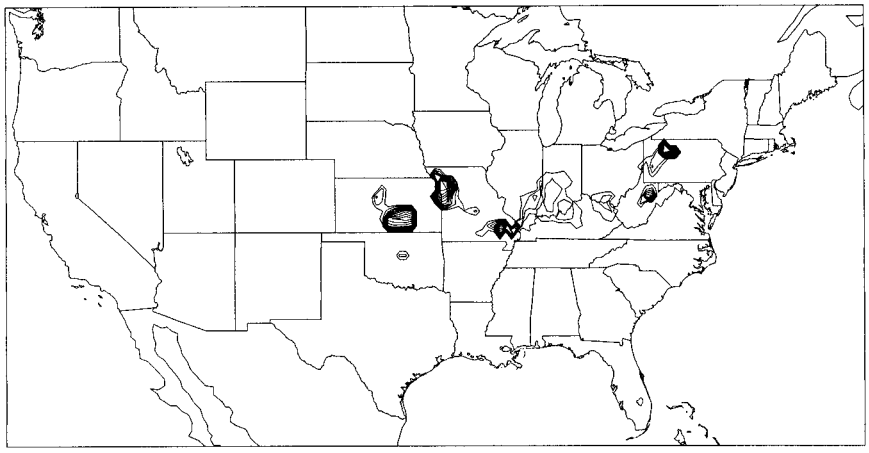

FIG. 4. Perturbation sea level pressure field (hPa) associated with cold pools after combining the bandpass sea level pressure field with the national multisensor precipitation analysis. Contour interval is 0.25 hPa.

Unauthenticated | Downloaded 05/11/21 01:50 AM UTC

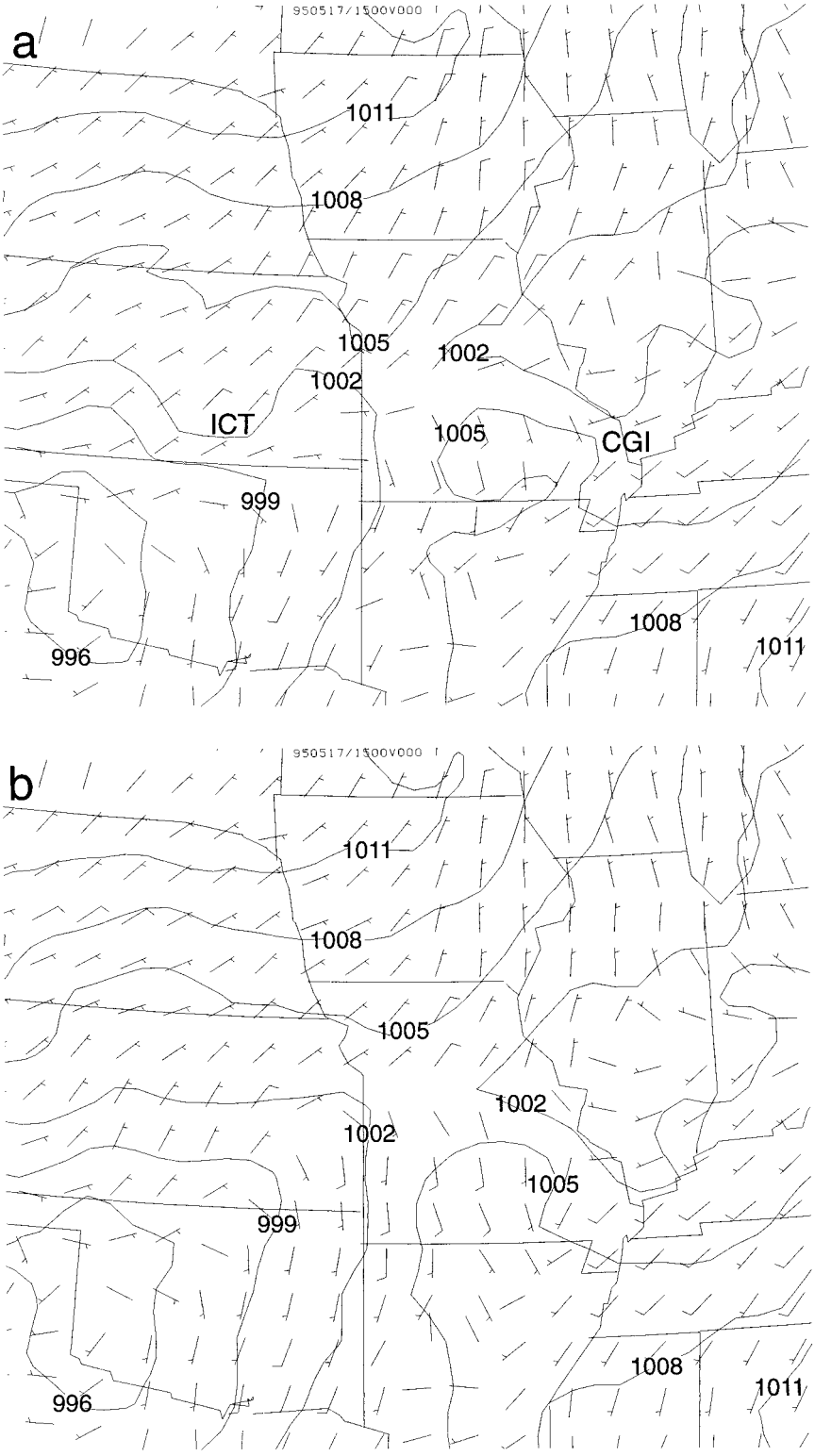

FIG. 5. Sea level pressure field (hPa) and 10-m winds from the Eta-29 initial condition using (a) cold pool initialization and (b) control initialization valid at 1500 UTC 17 May 1995 after the 3-h EDAS. Observations (c) using standard surface station plot with outflow boundaries denoted with the double-dashed lines [analysis convention from Young and Fritsch (1989)]. Winds are

Unauthenticated | Downloaded 05/11/21 01:50 AM UTC

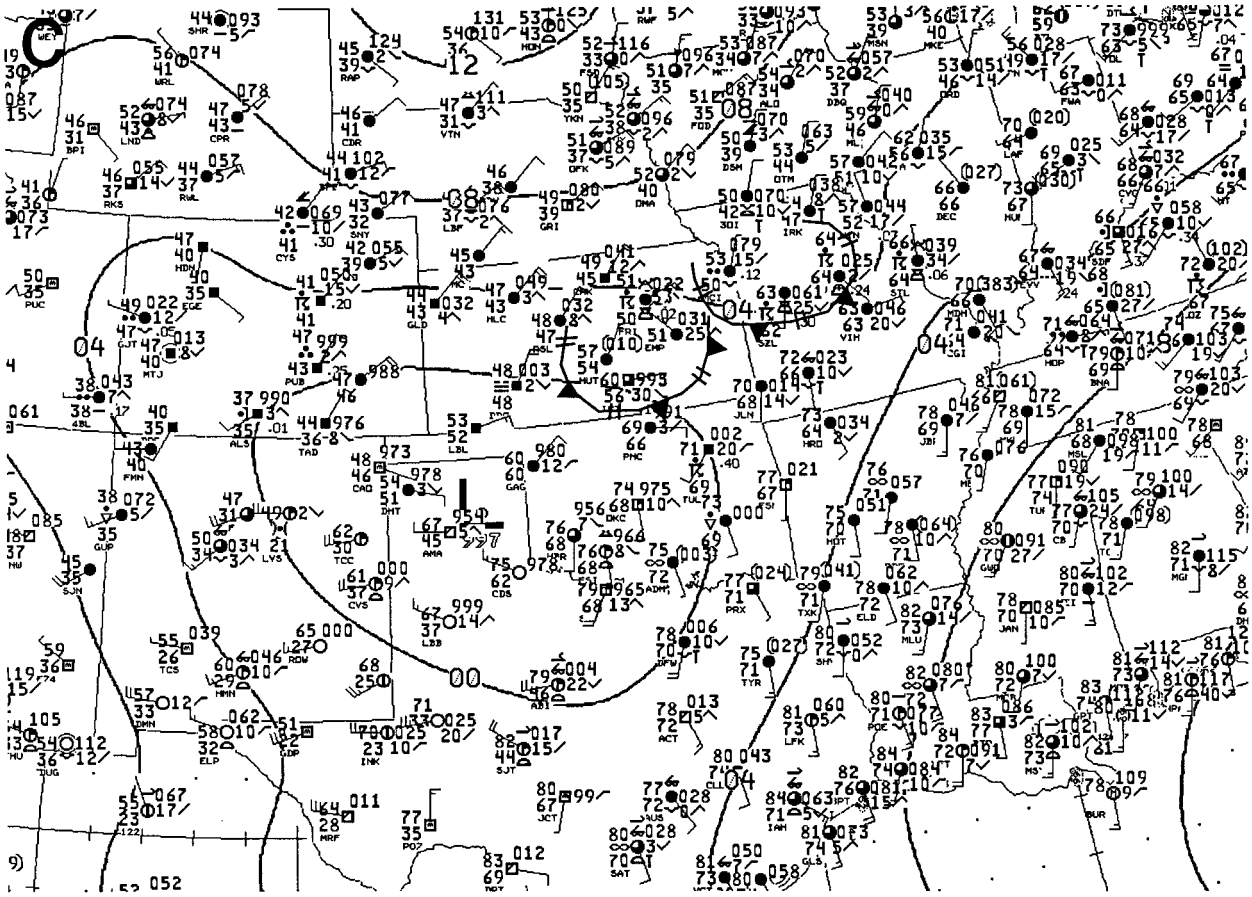

FIG. 5. (*Continued*) plotted every 80 km and a full wind barb is 5 m s^{-1}. Note the higher sea level pressures in south-central Kansas and eastern Missouri in (a) along with the modified wind field in this same region that indicate the effects of the cold pool initialization. Locations of Wichita (ICT) and Cape Girardeau (CGI) are also indicated.

el. The model has 50 vertical layers from sea level to the model top at 25 hPa, although the number of layers above ground level at any given location varies based upon the surface pressure. Since the Eta has been run at a variety of grid spacings, we refer to this version of the model as the Eta-29. This model includes the following physical parameterization schemes.

1) Parameterized convection. An implicit Betts–Miller–Janjic convective parameterization scheme is used to simulate the effects of convection (Betts 1986; Betts and Miller 1986; Janjic 1994). In simplified terms, the scheme searches for grid points where the atmosphere is conditionally unstable and, given that condition, will generate convection if sufficient moisture is available throughout the depth of the cloud. The minimum cloud depth needed to activate the scheme is 290 hPa, and if this depth condition is not met a shallow nonprecipitating scheme is activated that moves the atmosphere toward a mixing line structure between cloud base and cloud top. Given that deep convection occurs, the scheme constructs reference profiles of temperature and specific humidity based upon typical profiles determined from observational studies (Betts 1986). These profiles are then adjusted to satisfy a total enthalpy constraint.

   In general, the Betts–Miller–Janjic scheme is designed to respond well to sustained large-scale forcing in the presence of conditional instability and it is not likely to fail egregiously (see Kain et al. 1998). The scheme is not designed, however, to respond quickly to regions of strong mesoscale forcing, such as a cold pool, since it is only indirectly influenced by the effects of vertical motion. In addition, the scheme as implemented within the Eta Model does not include the effects of convective downdrafts and is unable to produce or contribute to the maintenance of cold pools.
2) Planetary boundary layer and surface physics. The model incorporates a 1.5-order turbulent kinetic energy scheme that is described by Mellor and Yamada (1982) and Janjic (1994). The land surface package includes two soil layers and incorporates the effects of vegetation through a canopy resistance treatment

Unauthenticated | Downloaded 05/11/21 01:50 AM UTC

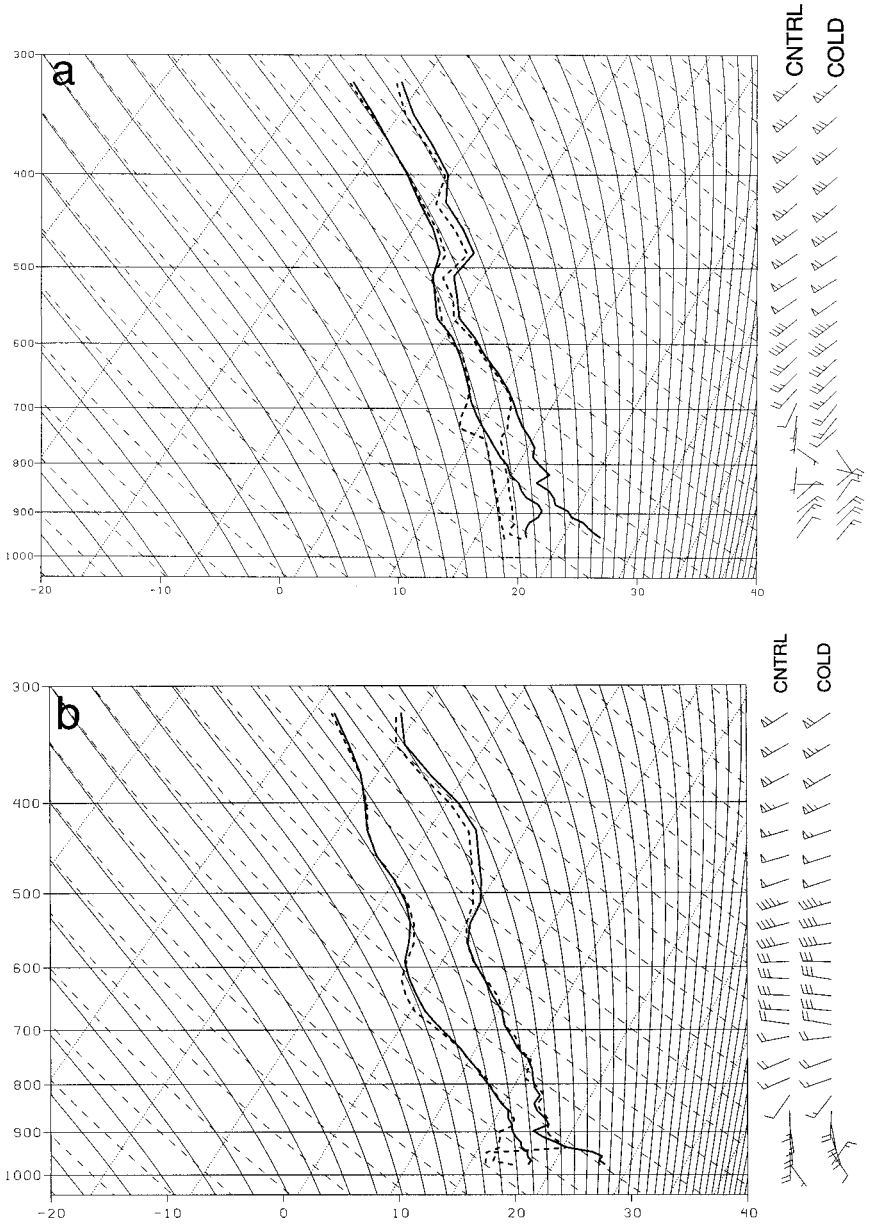

FIG. 6. Skew *T*–log*p* plots of vertical model soundings from (a) ICT and (b) CGI, from both the cold pool (dashed line) and control (solid line) Eta-29 runs valid at 1500 UTC 17 May 1995 after the 3-h EDAS. Full wind barb is 5 m s^{-1} and are indicated on the right of the diagram. Locations of ICT and CGI shown in Fig. 5a.

originally developed by Pan and Mahrt (1987) and extended by Chen et al. (1996). The fraction of green vegetation within each grid cell is determined from a monthly database of the annual cycle (with 0.15° horizontal spacing) derived from satellite measurements of the normalized differential vegetation index over a 5-yr period (Gutman and Ignatov 1998).

3) Explicit microphysics. Cloud liquid water and cloud ice are explicitly predicted using a single equation for cloud mixing ratio (Zhao et al. 1997). This scheme includes the effects of evaporation, condensation, and melting. Condensation occurs for relative humidities above 75% over land and above 80% over the ocean in order to account for the subgrid variations of the temperature and moisture fields. The cloud fields produced by this scheme influence the radiation calculations, providing a direct feedback between clouds and the land surface energy budget.

4) Initialization and data assimilation. The model is initialized using the Eta Data Assimilation System (EDAS) (Black 1994; Rogers et al. 1996). This pro-

Unauthenticated | Downloaded 05/11/21 01:50 AM UTC

cedure begins by interpolating a 6-h forecast from the global spectral model, valid at either 0000 or 1200 UTC, to the Eta-29 grid as a first guess field. This first guess field is then updated with all available observations using a regional optimum interpolation system (DiMego 1988; Rogers et al. 1995) to produce a static initial condition for the Eta-29. An EDAS is then conducted, in which a 3-h Eta-29 forecast is produced and new data are assimilated into the model fields at the end of this 3-h period (either 0300 or 1500 UTC). This process is referred to as the control Eta-29 model initialization and is identical to that used by the Mesoscale Eta Model. After this 3-h EDAS, a 33-h model forecast is produced. In order to include cold pools in the model initial conditions, a procedure must be designed to identify cold pools and insert them within the initial conditions.

3. Cold pool identification

Although a human-generated mesoscale analysis likely remains the best approach for identifying cold pools, a more algorithmic approach would be of great value in an operational setting. Therefore, an automated procedure to identify cold pools in the available observations is developed. With the nearly 400-km separation between upper-air observing sites, a distance far larger than the horizontal extent of most cold pools, the routine identification of cold pools has to be based upon other data sources. Although data from the Weather Surveillance Radars-1988 Doppler (WSR-88Ds), satellites, and radar wind profilers may be useful in defining the location of cold pools, and occasionally their depth, these data are not always able to observe cold pools, owing to data coverage or cloud obstruction problems. The data with the most uniform coverage that can be used to estimate regularly both the cold pool location and depth are the routine surface observations. But even with this much denser surface network, in which the observing stations are separated by an average of 65 km, cold pools are often sampled at only a handful of stations. However, even with these limitations, the surface data remain the best data source for identifying cold pools and are the foundation of the cold pool identification scheme. The other available observations are used to help define the horizontal extent of the cold pools.

In Stensrud and Fritsch (1994a), cold pools are identified by constructing two different hand analyses of the sea level pressure field: one that includes the surface stations within the cold pool, and one that does not. By manually subtracting these two analyses, a perturbation sea level pressure field associated with the cold pool is determined. To identify cold pools automatically, a similar procedure is constructed using an objective analysis approach. The process begins by producing an objective analysis of the sea level pressure field that retains mainly the large-scale wavelengths. This analysis uses a two-

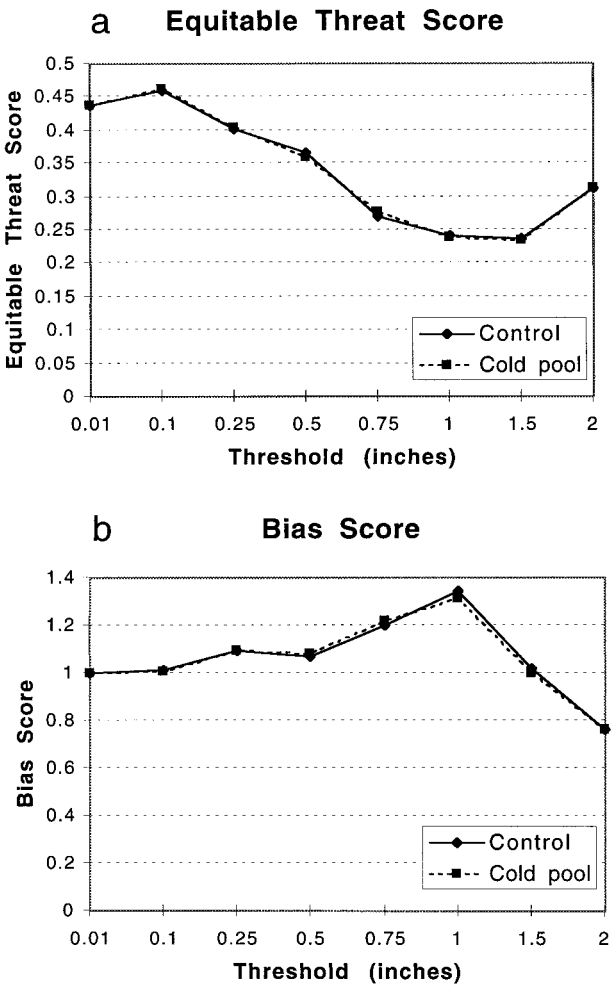

FIG. 7. Plots of (a) the equitable threat score and (b) the bias for 24-h precipitation forecasts from the control and cold pool initializations of the Eta-29. Precipitation thresholds are in inches.

pass Gaussian weight function scheme developed by Barnes (1964, 1973), in which the first-pass field of the gridded values for some parameter f are obtained by

$$f_o(i, j) = \sum_{n=1}^{N} w_n f_n(x, y) \Big/ \sum_{n=1}^{N} w_n, \qquad (3.1)$$

where f_o is the gridded value of f at some location (i, j) on the grid, f_n is the observed value of f at some location point (x, y), N is the total number of observations, and w_n is the weight function defined as

$$w_n = e^{(-d_n^2/4c)}, \qquad (3.2)$$

where d_n is the distance from the (i, j) grid point to the observed data location (x, y), and c is an arbitrary parameter chosen to obtain the desired response. Barnes (1973) shows that the response function for this functional is

$$R_o = e^{(-4\pi^2 c/L^2)}, \qquad (3.3)$$

Unauthenticated | Downloaded 05/11/21 01:50 AM UTC

FIG. 8. Difference in total precipitation forecasts (in.) between the cold pool and control initialization forecasts at 24 h, valid 1200 UTC 18 May 1995. Differences calculated by subtracting the control precipitation total from the cold pool precipitation total, such that negative values indicate the cold pool run produces less precipitation. Shading used for values below −0.1, −0.2, −0.4, and −0.6 in. as shown in the key at the left. The thick black line is the zero contour.

where L is the wavelength. A single correction pass can be used to better fit the analysis to the data. This is done by calculating the difference D_n between the observations and the analysis for each observation, such that

$$D_n(x, y) = f_n(x, y) - f_o(x, y), \tag{3.4}$$

where $f_o(x, y)$ is calculated from $f_o(i, j)$ using a bilinear interpolation scheme. A second analysis is then conducted to produce the final analysis $f(i, j)$, in which

$$f(i, j) = f_o(i, j) + \sum_{n=1}^{N} w_n' D_n \Big/ \sum_{n=1}^{N} w_n' \tag{3.5}$$

and

$$w_n' = e^{(-d_n^2/4gc)}, \tag{3.6}$$

where g is an arbitrary parameter chosen for the modified weight function w_n'. The final wavelength dependent response function is then

$$R = R_o(1 + R_o^{g-1} - R_o^g). \tag{3.7}$$

Values of $c = 4320$ km^2 [(66 km)^2] and $g = 0.3$ are used for the large-scale analysis. An analysis that contains more of the mesoscale structure is obtained using the identical approach, but with values of $c = 4320$ km^2 and $g = 0.8$. The change in the value of g is sufficiently large enough to modify the response in order to capture both the large-scale and mesoscale features. As discussed by Barnes (1973), Doswell (1977), and Maddox (1980), the difference between two separate low-pass analyses, called a bandpass analysis, can be used to maximize the details in a desired wavelength range. Therefore, the large-scale analysis ($g = 0.3$) is subtracted from the mesoscale analysis ($g = 0.8$) to filter out the large-scale wavelengths and define only the mesoscale component of the sea level pressure field (Fig. 1) (Doswell 1977). This bandpass field is then restored to 100% amplitude at the 250-km wavelength, where the maximum response difference occurs (Fig. 1).

In order to capture a cold pool, a feature often on the order of 100–400 km in horizontal extent, the mesoscale objective analysis necessarily includes wavelengths near the Nyquist frequency and contains a mixture of both noise and the observed mesoscale-sized pressure perturbations (see Fig. 2). This unfortunate consequence of the near match between the surface observing network spacing of 65 km and the typical cold pool size (100–400 km) requires some method for removing the noise from the perturbation pressure analysis before it can be used as a basis for inserting cold pools into model initial conditions. Since cold pools that are large enough to be sampled by the surface data are produced by the processes associated with organized convective activity

Unauthenticated | Downloaded 05/11/21 01:50 AM UTC

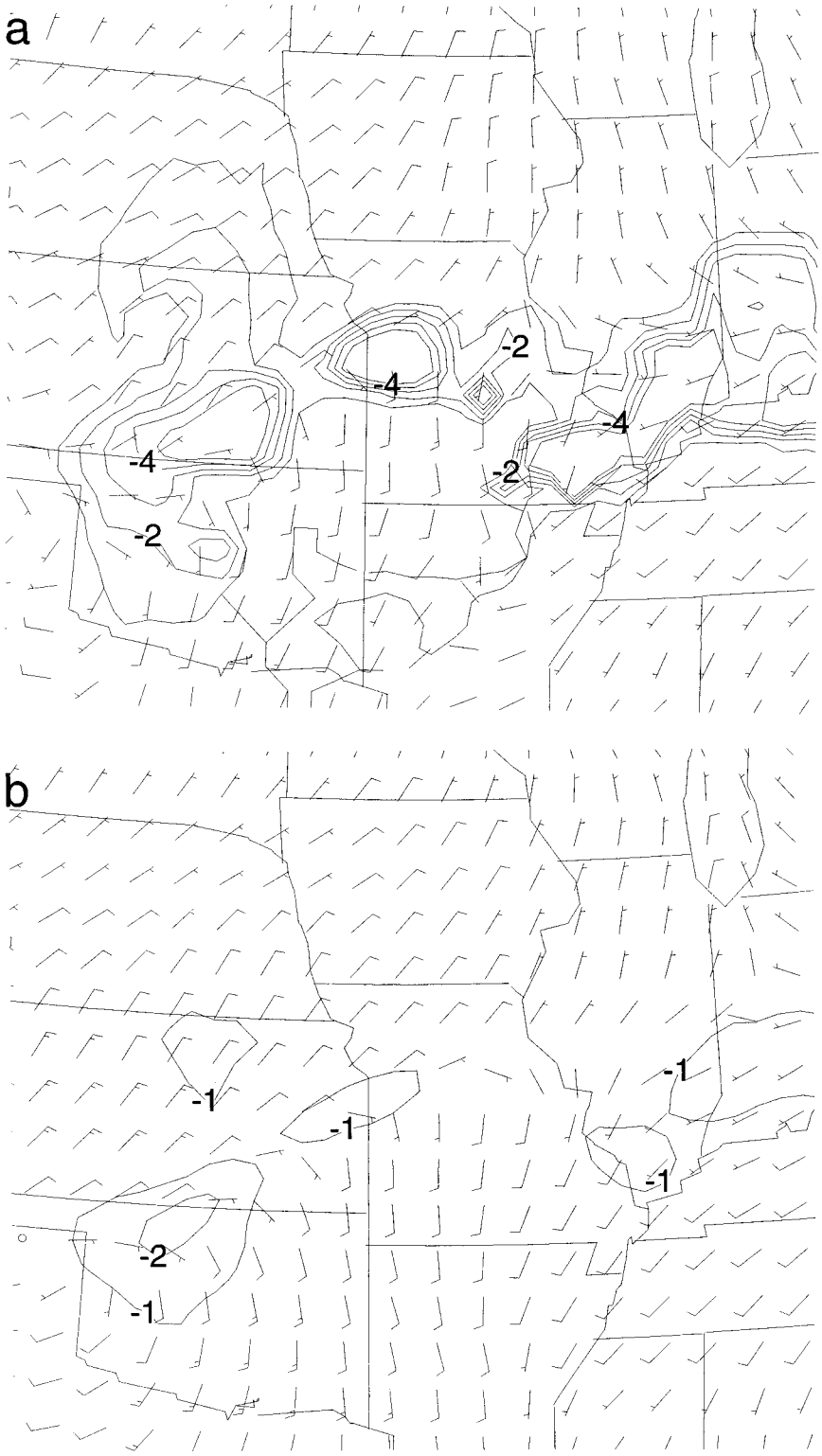

FIG. 9. Differences in 2-m temperatures (°C) from the cold pool and control runs valid at (a) 3, (b) 6, and (c) 9 h into the model runs started at 1200 UTC 17 May 1995. Negative values indicate that the cold pool run is colder than the control run. Contour interval of 1°C in (a) and

Unauthenticated | Downloaded 05/11/21 01:50 AM UTC

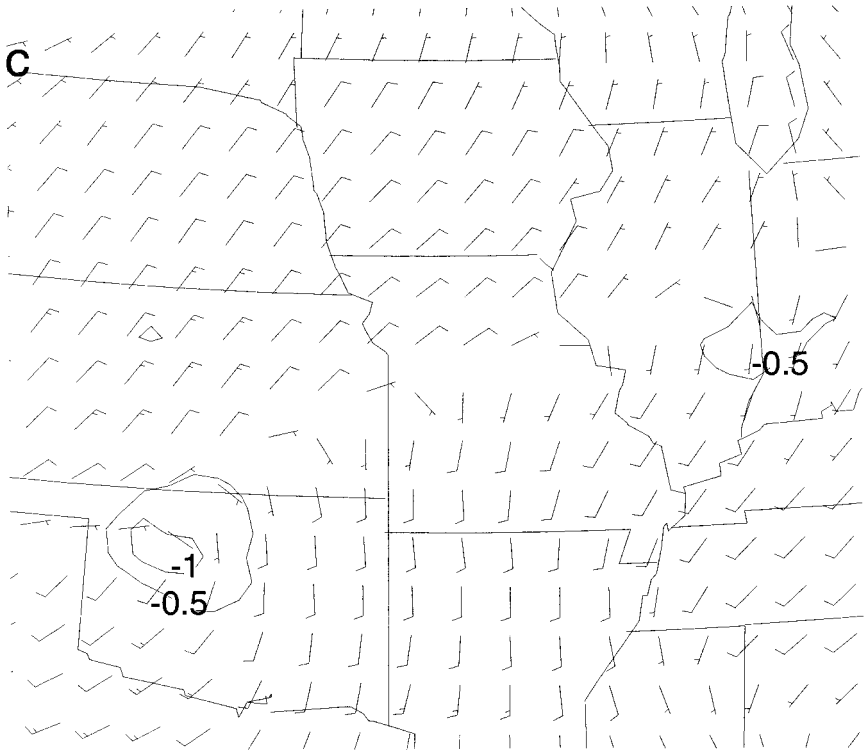

FIG. 9. (*Continued*) (b), while the contour interval is 0.5°C in (c). Wind vectors are from the control initialization forecast and are plotted every other grid point. Full wind barb is 5 m s^{-1}.

(typically MCSs during the warm season), the hourly multisensor national precipitation analysis (Fig. 3) produced by NCEP (Baldwin and Mitchell 1996) can be used to delineate the positive sea level pressure perturbations associated with precipitation from those associated with noise and other meteorological features. This multisensor analysis uses both hourly rain gauge and WSR-88D precipitation estimates. Only those locations that both have a positive sea level pressure perturbation and are surrounded by regions of precipitation are identified as having a cold pool at the surface (Fig. 4). For this study, only a single hourly national precipitation analysis is used, owing to data availability, although a composite over several hours (possibly using a minimum precipitation amount threshold) would likely produce a more representative cold pool. Additional information from the WSR-88Ds, satellite, and radar wind profilers could be used to further refine the cold pool positions and depths, although these data are not used in the present exploratory study. The objectively analyzed bandpass pressure perturbations associated with the cold pools are then stored along with their corresponding latitude and longitude location on a 50-km grid defined across the contiguous 48 states.

Seventeen cold pool cases during 1995 have been identified and objectively analyzed using the cold pool algorithm. Results indicate that this procedure can capture the location and magnitude of cold pools as indicated by a comparison with hand analyses of the surface data (not shown). While this algorithm is unable to capture cold pools of less than 100 km in length, it is successful at capturing the largest and strongest cold pools detected in the surface data. Therefore, it is used to calculate the perturbation sea level pressure needed to initialize cold pools within the Eta Model.

4. Cold pool initialization

Once the cold pools are identified, the final step is to use the output from the cold pool identification algorithm to insert the cold pools into the Eta-29 initial conditions. Fujita (1959) and Wakimoto (1982) conclude that the pressure rise behind the gust front, the leading edge of a cold pool, is due to the increased hydrostatic pressure of the cold air. Thus, knowledge of the surface pressure perturbation and the virtual temperature of the cold pool can be used to determine the depth of the cold air as shown by Stensrud and Fritsch (1994a). The cold pool surface temperature within the Eta-29 initial condition is estimated by bringing a parcel from 300 hPa above the surface down to the surface by moist-adiabatic descent. This is a crude estimate of downdraft temperature and results indicate that the outflows produced by this scheme are typically too cold by 1°–2°C. However, owing to the difficulty of maintaining the cold pool in the Eta Model, discussed below, this

Unauthenticated | Downloaded 05/11/21 01:50 AM UTC

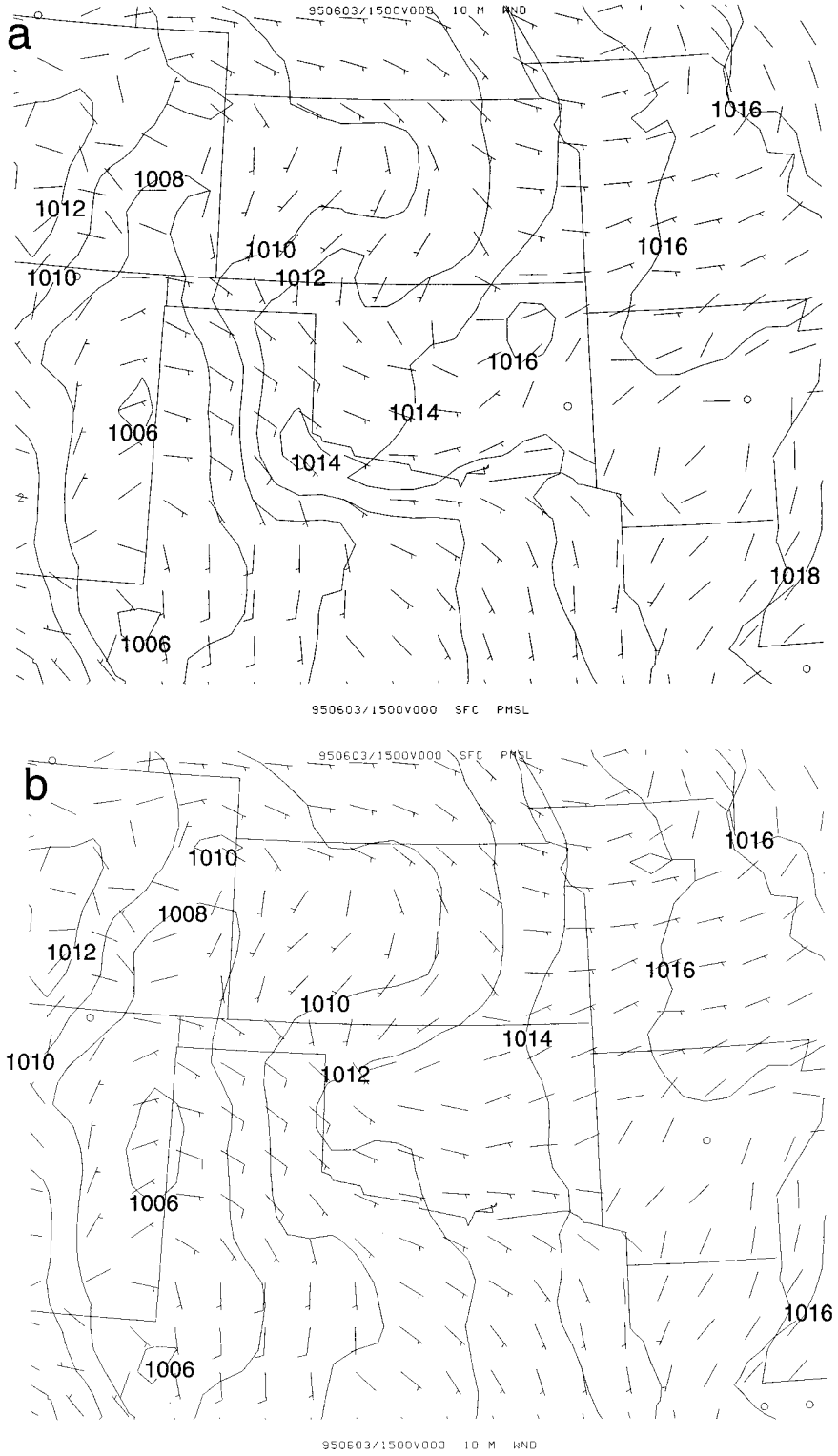

FIG. 10. Sea level pressure field (hPa) and 10-m winds from the Eta-29 initial condition using (a) cold pool initialization and (b) control initialization valid at 1500 UTC 3 Jun 1995 after the 3-h EDAS. Observations from 1200 UTC 3 June 1995 (c) using standard surface station plot

Unauthenticated | Downloaded 05/11/21 01:50 AM UTC

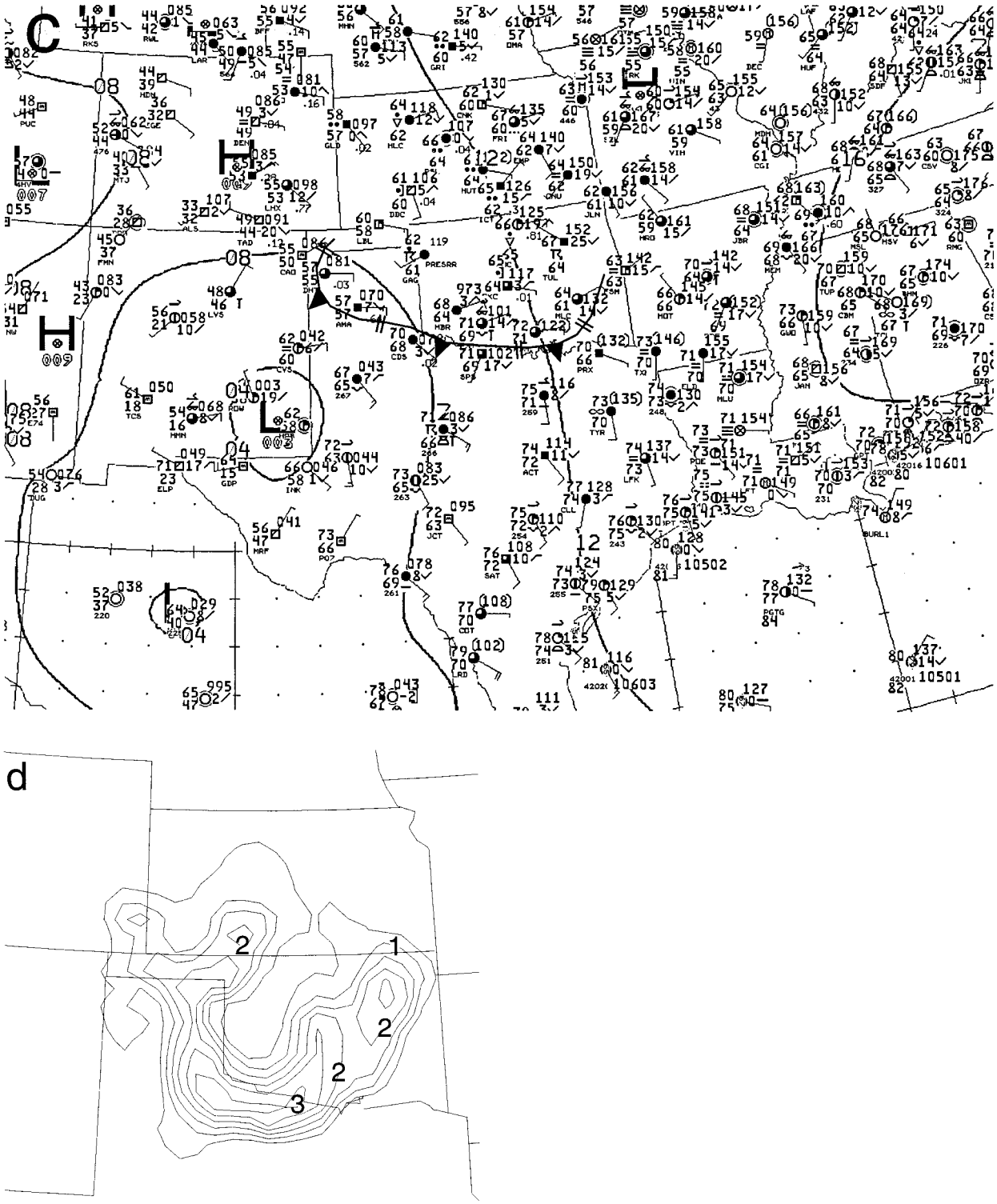

FIG. 10. (*Continued*) with outflow boundaries denoted with the double-dashed lines (plots from 1500 UTC are unavailable). Winds are plotted every 80 km and a full wind barb is 5 m s^{-1}. Sea level pressure perturbation (hPa) produced by the cold pool initialization scheme (d) at 1500 UTC 3 June 1995.

Unauthenticated | Downloaded 05/11/21 01:50 AM UTC

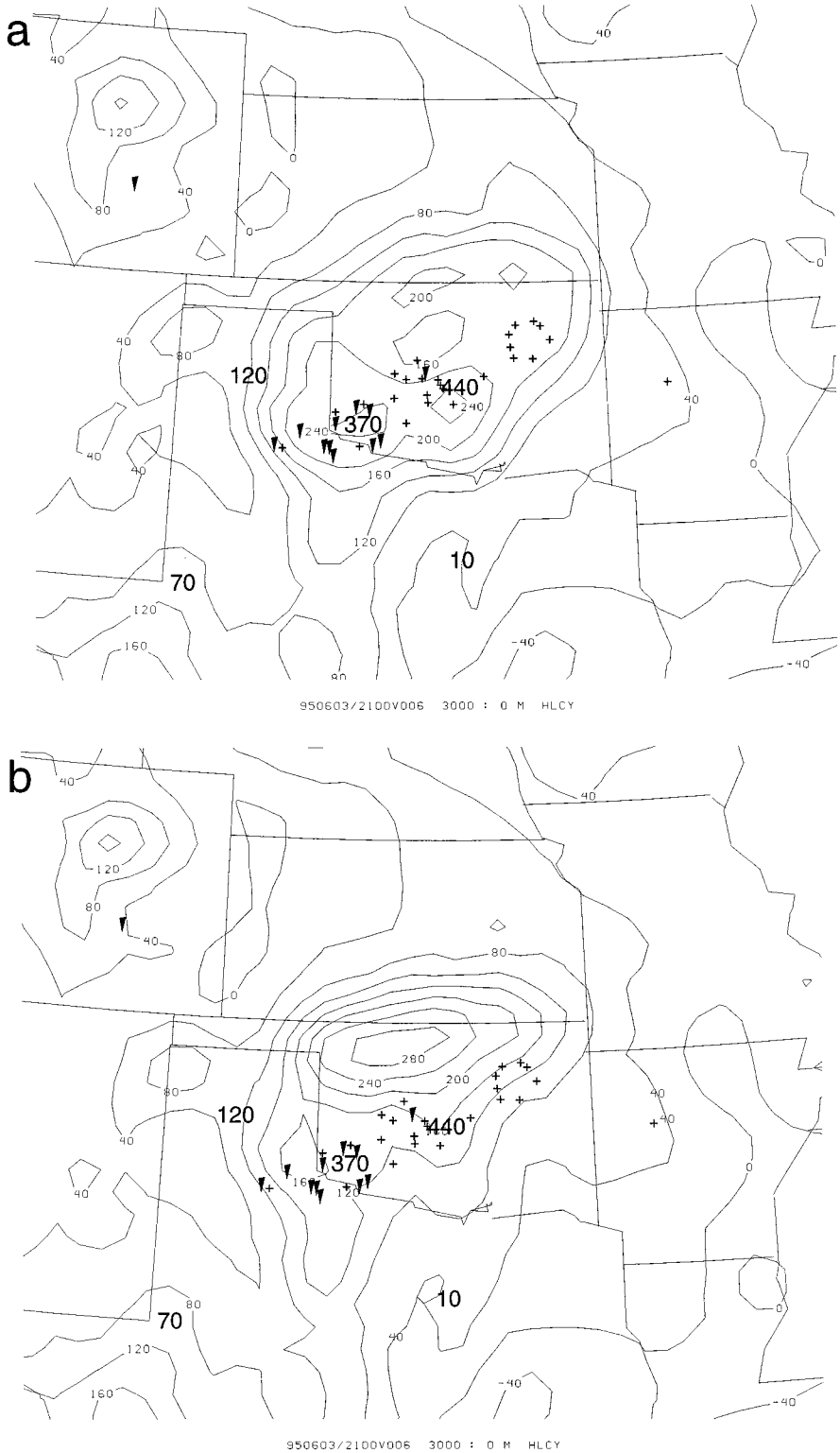

FIG. 11. SREH ($m^2 s^{-2}$) from (a) cold pool run and (b) control run at 6 h into the model forecasts valid 2100 UTC 3 Jun 1995. Contour interval is 40 $m^2 s^{-2}$. Numbers in bold indicate SREH values calculated from the VORTEX special soundings. An inverted triangle indicates the location of a tornado report, while a + indicates the location of a severe wind report.

Unauthenticated | Downloaded 05/11/21 01:50 AM UTC

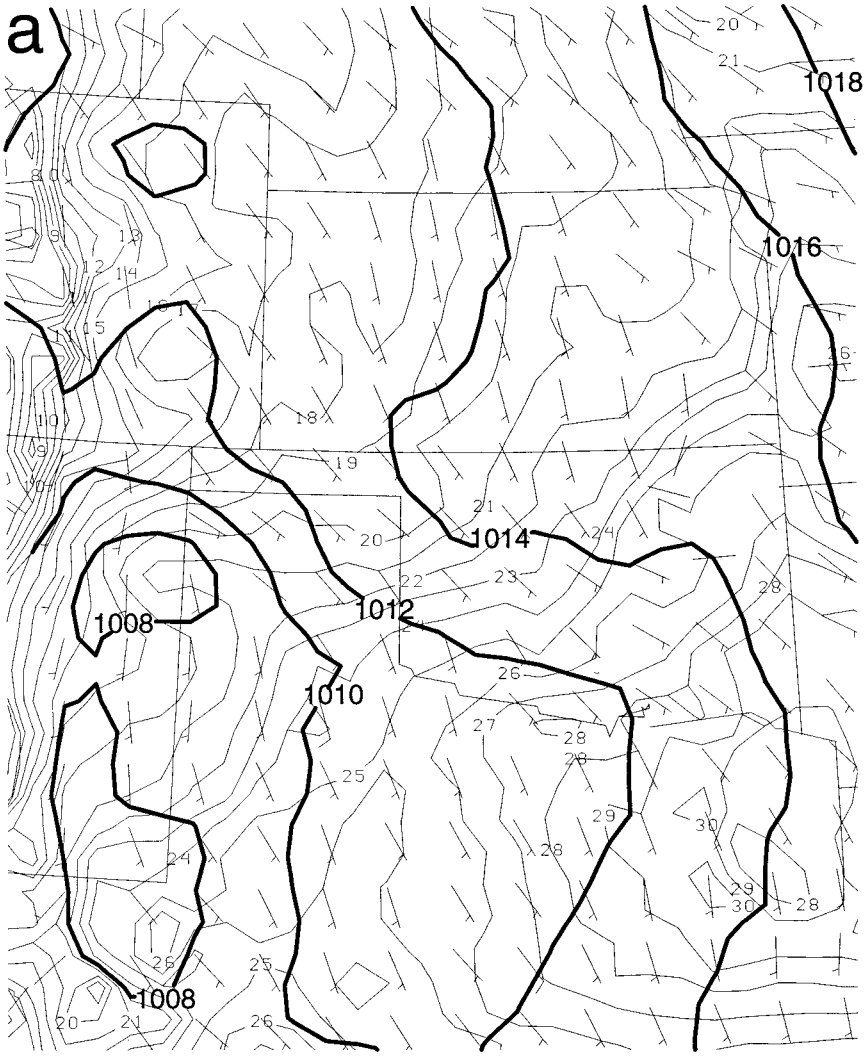

FIG. 12. Sea level pressure field (hPa), 2-m temperature field (°C), and low-level winds from the Eta-29 initial condition using (a) cold pool initialization and (b) control initialization from the 12-h forecasts valid at 0300 UTC 4 Jun 1995. Observations (c) using standard surface station plot

simplification is deemed acceptable since it likely assists in increasing the longevity of the cold pool in the model. Once the cold pool surface temperature is defined, the hypsometric equation is used to build a cold pool upward from the ground surface in the model initial condition. The cold pool temperature profile is assumed to follow a moist adiabat and the relative humidity is arbitrarily held constant at 80%. The top of the cold pool is defined as the model level where the perturbation pressure due to the cold pool equals that calculated by the bandpass objective analysis.

The initialization of the wind field within the cold pool is another concern. Unlike Stensrud and Fritsch (1994a), who initialized both the momentum and thermodynamic fields within the cold pool, in this study the wind fields are not modified within the cold pool region. Although divergent wind fields are frequently observed within cold pools (Fujita 1959; Stensrud and Maddox 1988; Schmidt and Cotton 1989), the ability to automatically define a reasonable three-dimensional wind field from the available data is limited. However, within the shallow, stratified cold pool region, the wind field should adjust to the mass field (Blumen 1972; Fritsch et al. 1992). Therefore, this cold pool initialization procedure is added as a special pre- and postprocessor to the control data assimilation system for the Eta-29, where the cold pool is inserted into the model initial conditions both before and after a 3-h data assimilation period. This technique should help develop the wind field within the cold pool during the data assimilation time period (see Fig. 5).

Two soundings from within the cold pool region after the 3-h data assimilation period from both the control and cold pool Eta-29 forecasts illustrate the variety of

Unauthenticated | Downloaded 05/11/21 01:50 AM UTC

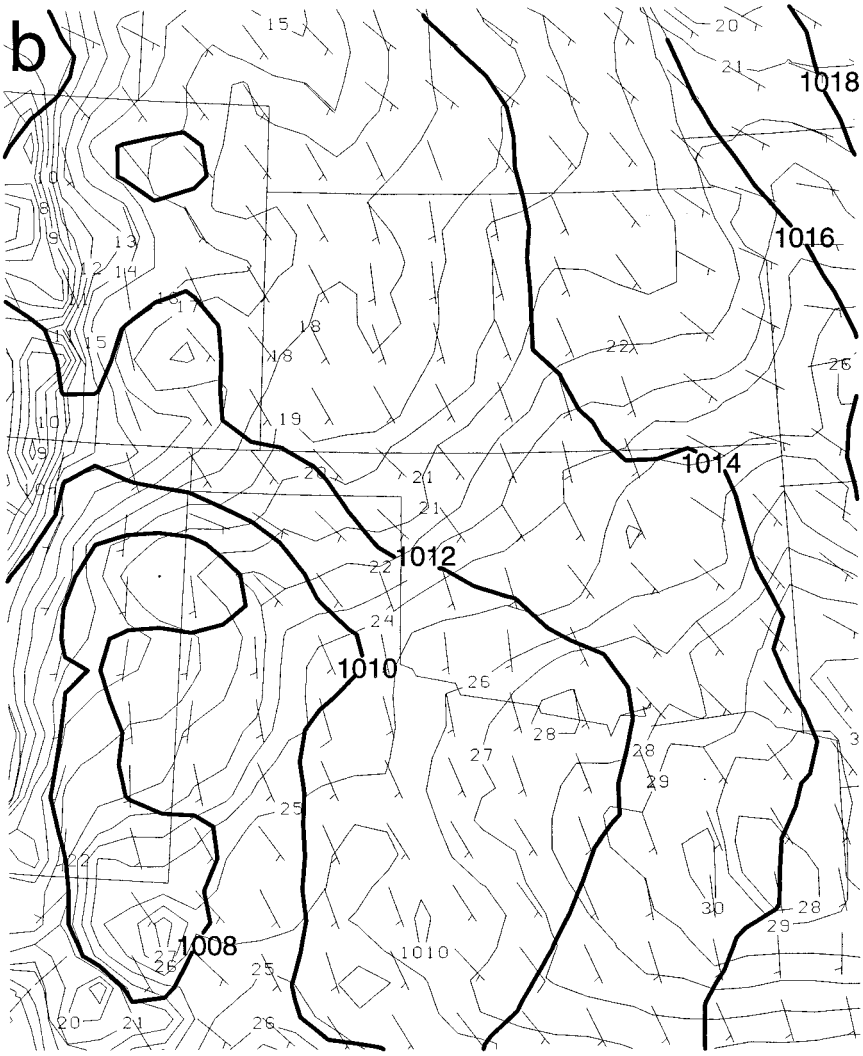

FIG. 12. (*Continued*) with temperatures contoured at 20° and 24°C. Winds are plotted every 80 km and a full wind barb is 5 m s^{-1}.

cold pool structures that can be created by the cold pool initialization (Fig. 6). The Wichita soundings show a cold pool that extends up to approximately 750 hPa, owing to the moist midlevel air used to estimate the cold pool temperature profile (Fig. 6a). In contrast, the Cape Girardeau soundings show a very shallow cold pool (Fig. 6b). This is due to both the smaller cold pool pressure perturbation analyzed at Cape Girardeau in comparison with the pressure perturbation at Wichita, and the relatively dry midlevels at Cape Girardeau that allow for a colder cold pool temperature profile. Both of the soundings initialized within the diagnosed cold pool region resemble soundings observed within actual cold pools (Fujita 1959; Wakimoto 1982), suggesting that the simple cold pool initialization produces realistic structures. Other differences seen in the control and cold pool soundings, including the slightly different wind and temperature profiles throughout the troposphere, are in response to differences in the model predictions during the 3-h data assimilation period. In particular, the low-level winds at Cape Girardeau are northeasterly in the cold pool run in comparison to the southeasterly winds in the control Eta-29 run. Results from the control and cold pool forecasts are now examined more closely to determine the importance of the cold pools to the subsequent evolution of the model forecasts.

5. Eta Model results

The cold pool scheme is used to initialize the Eta-29 for seven different times over 6 days during 1995 for which significant cold pools are seen in the observations (see Table 1). Most of these cases have significant large-scale forcing for upward motion, as diagnosed kinematically from an objective analysis of the standard rawinsonde data. The weakest case is 3 June 1995 where

Unauthenticated | Downloaded 05/11/21 01:50 AM UTC

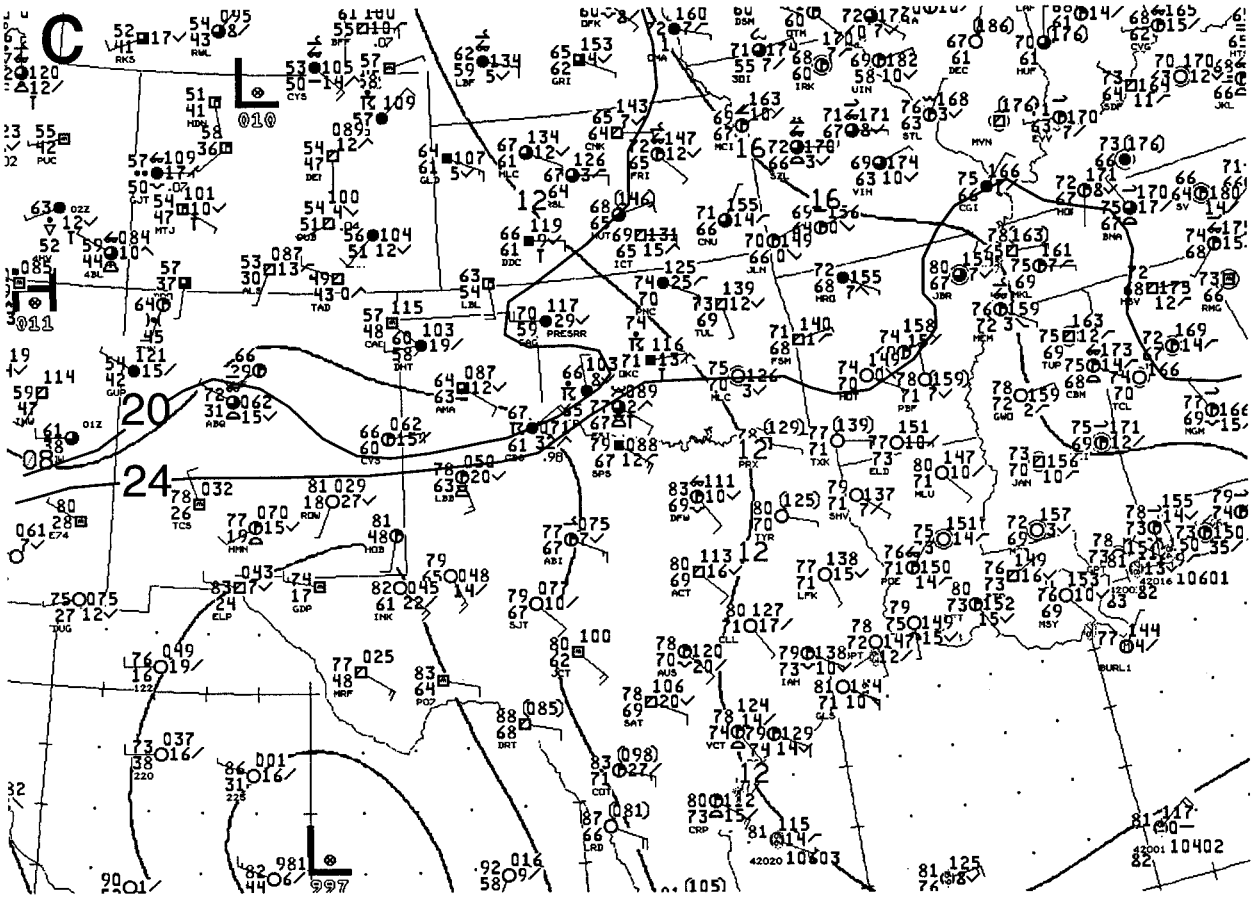

FIG. 12. (*Continued*).

the minimum values of omega near the cold pool region are only -2.8 μb s^{-1}, which still is not weakly forced as defined by Stensrud and Fritsch (1994b). However, of all the forecast cases this one is the most likely to show an appreciable effect of the cold pool, since mesoscale forcing appears to play a more important role in more weakly forced systems.

Calculations of the equitable threat score and bias (Wilks 1995) over the entire United States from all the cases suggest that the cold pool initialization has little effect on the precipitation field within the Eta-29 as compared to the forecasts without the cold pool (Fig. 7). In essence, the inclusion of the cold pool shifts the precipitation axis slightly in most cases, but does not have a major effect on the model forecast of precipitation, with 24-h precipitation totals typically well within 1 in. from the values forecast from the control initialization (see Fig. 8). In addition, the general pattern of convection from the cold pool initialization run is very similar to the operational run.

TABLE 1. Days and times of model initial conditions and minimum values of omega near cold pool region between the surface and 500 hPa calculated kinematically.

Time and date of model initial condition	Omega (μb s^{-1})
0000 UTC 23 Apr	-4.5
00000 UTC 8 May	-5.4
0000 UTC 17 May	-4.8
1200 UTC 17 May	-5.5
1200 UTC 3 Jun	-2.8
0000 UTC 5 Jun	-5.0
0000 UTC 11 Jun	-4.4

The similarity between forecasts from the cold pool and control Eta-29 initializations is mainly due to the use of the Betts–Miller–Janjic convective scheme. The inclusion of the cold pool affects the calculations of cloud base and total column moisture, reducing the amount of precipitation produced by the convective scheme within the cold pool regions. However, the presence of the cold pool does not appear to significantly alter the region in which the convective scheme is activated. This is attributed to the cold pool initialization only reducing, and not eliminating, CAPE at the grid points within the cold pool. Since the large-scale forcing remains strong over the region, and positive CAPE is present, the ability of the convective scheme to activate is not influenced significantly by the cold pool. Changes

Unauthenticated | Downloaded 05/11/21 01:50 AM UTC

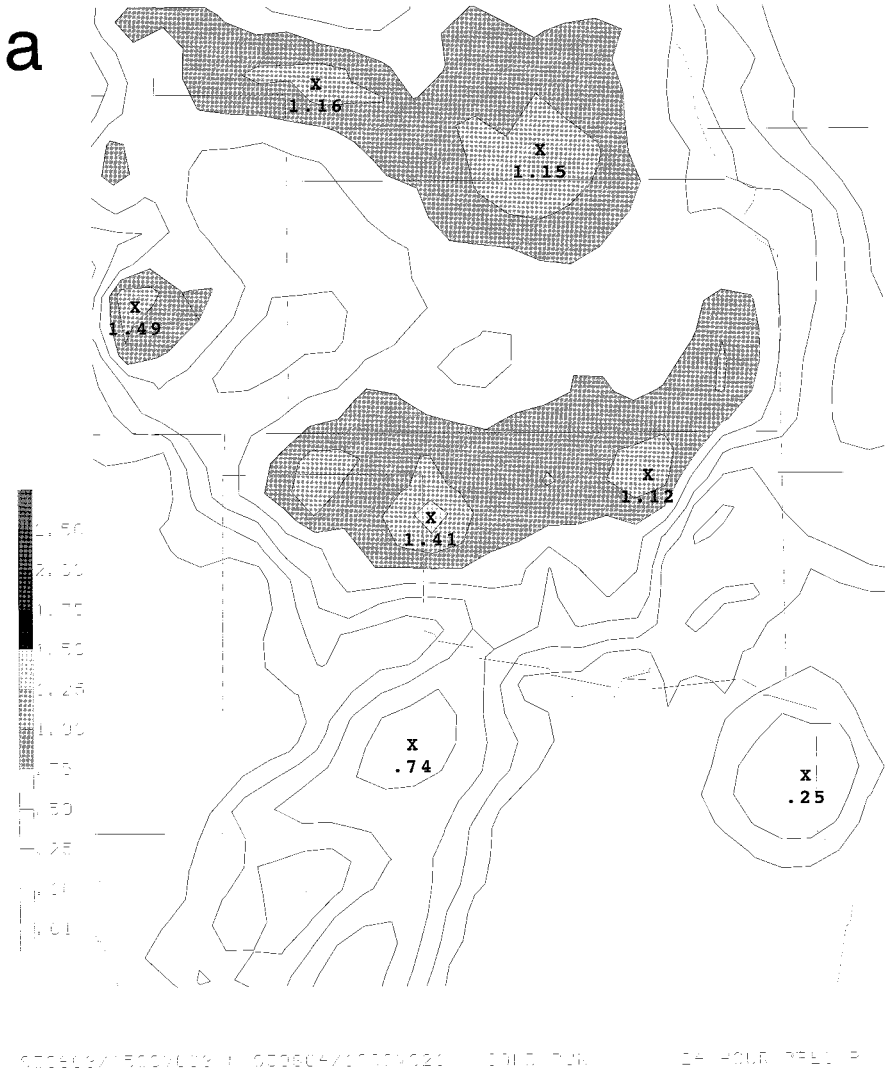

FIG. 13. Total 24-h precipitation (in.) from (a) cold pool run, (b) control run, and (c) observations. Model forecast precipitation contoured every 0.25 in., while the observations are contoured every 1 in. with a 0.50-in. contour also indicated.

outside of the cold pool regions are due to the nonlinear dynamical feedbacks of the cold pool on the model forecast.

The typical life span of the cold pool in the Eta-29 can be illustrated by examining the model forecast initialized at 1200 UTC 17 May 1995. Cold pools are identified by subtracting the cold pool Eta-29 run temperatures interpolated to the 2-m height above ground level from the control run temperatures at the same level (Fig. 9). While the cold pool regions are easily identified after the 3-h EDAS and the subsequent cold pool insertion, which occurs at 1500 UTC, by 6 h into the forecast the cold pool temperature perturbations have been reduced by a factor of 3 in most locations. This trend continues until by 9 h the cold pools are very weak and can hardly be identified. Common to all the model forecasts in relatively strong large-scale forcing is the development of convection in the model over the cold pool regions. The vertical mixing that occurs when the convective scheme is activated may contribute to the erosion of the cold pool, although the exact mechanisms that cause the cold pool to dissipate fairly rapidly have not been examined.

In several cases, small differences can still be seen at 24 h between the cold pool and control Eta-29 runs, but typically are only clearly seen in derived fields such as CAPE and SREH that are calculated over a vertical depth, in which the small changes found at each vertical level due to the cold pool can be accumulated. However, from a forecast perspective, the differences at 24 h between the cold pool and control Eta-29 initialization runs are not typically significant.

The one case in which the cold pool forecast is significantly different from the control Eta-29 run is the

Unauthenticated | Downloaded 05/11/21 01:50 AM UTC

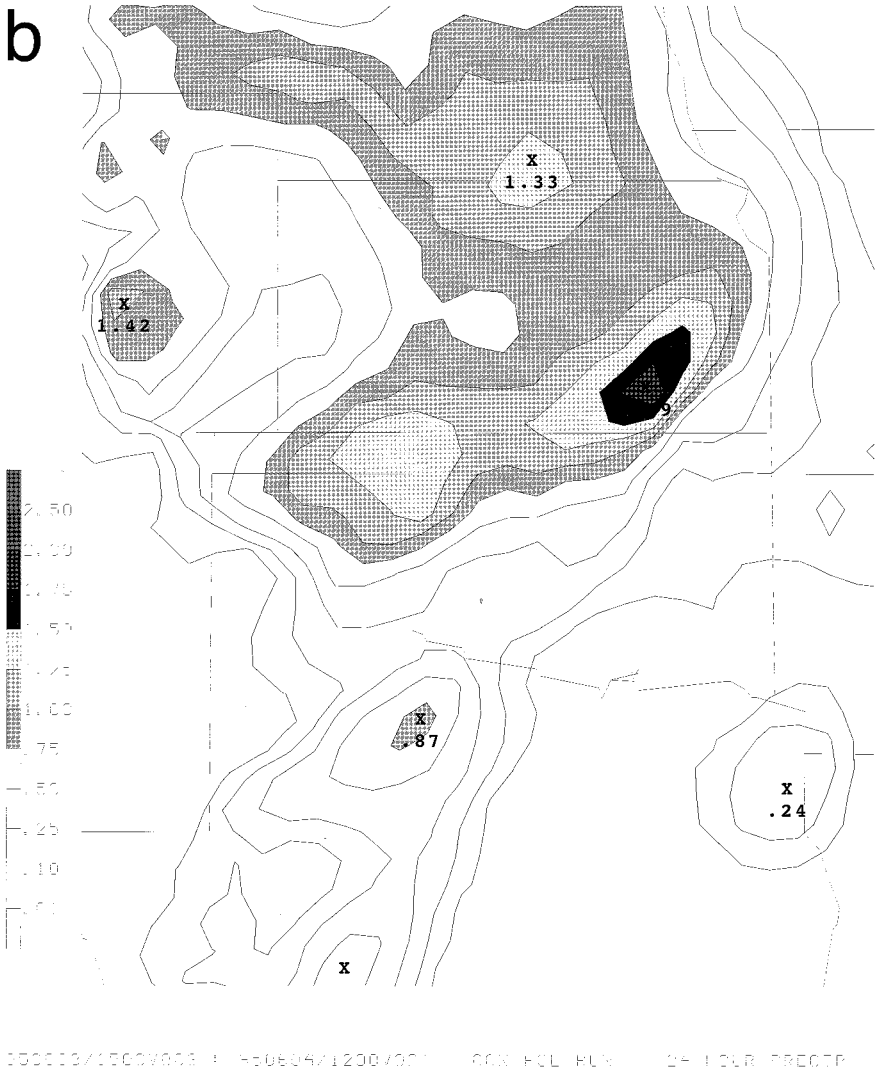

FIG. 13. (*Continued*).

more weakly forced case from 3 June 1995. Comparisons between the cold pool and control Eta-29 initializations after the 3-h EDAS show significant differences in the sea level pressure and low-level temperature and wind fields over Oklahoma and the Texas Panhandle at 1500 UTC (Fig. 10), even though the control initialization captured some aspects of the cold pool, as suggested by the higher sea level pressures in north-central Oklahoma. However, unlike the other forecasts examined, these differences persist in the cold pool run as can be easily seen in the calculated SREH fields at the 6-h forecast time (Fig. 11). Special soundings taken during the Verification of the Origin of Rotation in Tornadoes Experiment (VORTEX) (Rasmussen et al. 1994) indicate that the cold pool forecast captures the southward extent of the high SREH region in southwestern Oklahoma much better than the control Eta forecast, even though both forecasts underpredict the SREH values. Indeed, tornadic supercell thunderstorms did form on this day with 10 tornado reports near the southwestern corner of Oklahoma and high wind reports extending from southwestern Oklahoma northeastward (Fig. 11). The region in which the tornadoes were reported has SREH values above 240 $m^2\ s^{-2}$ in the cold pool forecast, but the SREH values are only slightly above 120 $m^2\ s^{-2}$ in the control Eta Model forecast. Since SREH has been found to be a useful field for assessing the threat of supercell thunderstorms (Davies-Jones et al. 1990), the difference in these forecasts is significant and illustrates the importance of cold pools in some situations.

The effects of the cold pool continue to influence the forecast through 12 h (0300 UTC 4 June) as seen in the sea level pressure and low-level temperature and wind fields (Fig. 12). The presence of the cold pool has increased the sea level pressure in central Oklahoma, cooled the temperatures, and backed the winds. While the sea level pressure values across Oklahoma from the

Unauthenticated | Downloaded 05/11/21 01:50 AM UTC

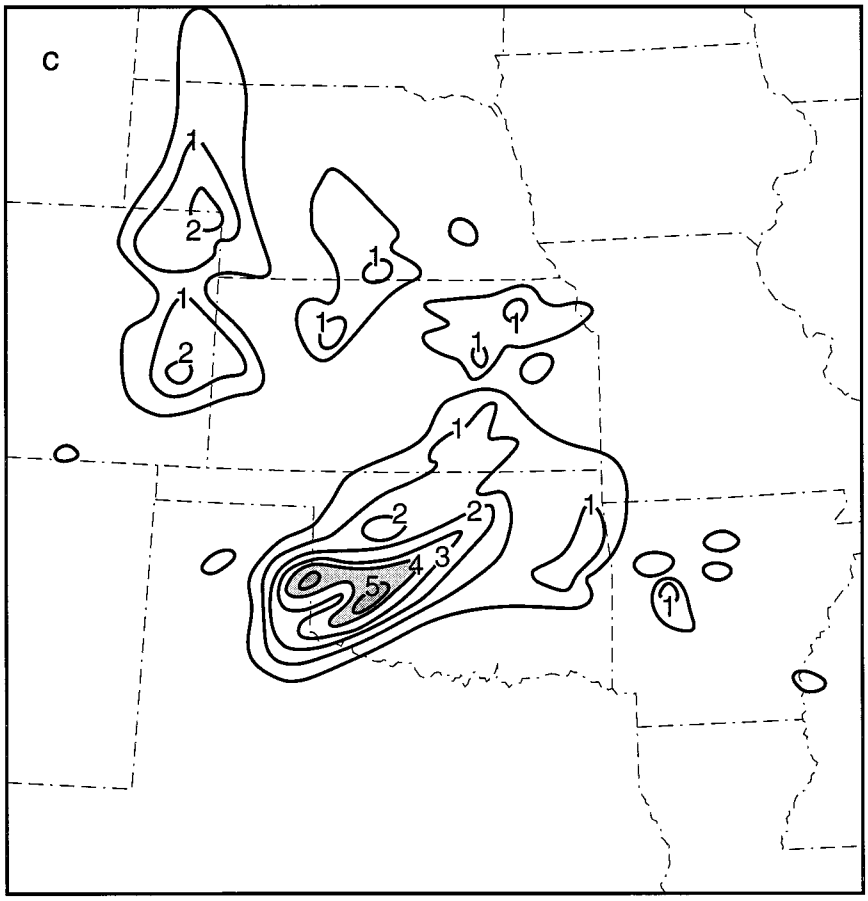

FIG. 13. (*Continued*).

cold pool run are higher than observed, the more easterly winds and the tighter temperature gradient in southern Oklahoma and the Texas Panhandle more closely match the observed values in this region than the control Eta Model forecast. It is also interesting to note that neither of the model forecasts develop convection over Oklahoma until after the 12-h forecast time, much later than seen in the other cases examined, thereby minimizing the influence of convective processes on the cold pool evolution.

The 24-h total rainfall fields, valid 1200 UTC 4 June 1995 (Fig. 13), are also influenced by the cold pool, with the region of heaviest rainfall shifted slightly southward from southern Kansas in the control Eta-29 run into central Oklahoma in the cold pool run. The observed 24-h rainfall totals (Fig. 12c) show that the rainfall amounts in Kansas are all below 2 in., whereas a region of rainfall exceeding 5 in. is reported in Oklahoma. Therefore, even with the Betts–Miller–Janjic convective scheme, a cold pool initialization is occasionally able to alter the precipitation forecasts as well. In addition, knowledge of the persistence of the cold pool would have been of value to forecasters issuing heavy precipitation forecasts.

6. Discussion

These results indicate that under strong large-scale forcing for upward motion, the presence of cold pools has little effect on the Eta-29 forecasts beyond 6 h and on the 24-h precipitation totals. This is due in part to the use of the Betts–Miller–Janjic convective parameterization scheme that responds well to sustained large-scale forcing when convective instability is present, yet does not respond directly to the presence of cold pools and is unable to develop or assist in the maintenance of cold pools owing to the lack of a downdraft parameterization. However, results from the one forecast made under a more weakly forced large-scale environment show that the model forecast is significantly altered when a cold pool is included in the model initial conditions. This result is consistent with the conclusions of Stensrud and Fritsch (1994b), who suggest that mesoscale features are most important in weakly forced synoptic situations. For these types of events, the incorporation of cold pools into operational weather prediction systems is a potentially important aspect in the creation of model initial conditions, and may lead to significant improvements in model forecasts during the

Unauthenticated | Downloaded 05/11/21 01:50 AM UTC

warm season. Observational evidence supports this viewpoint, since the importance of cold pools to the development and evolution of severe thunderstorms and heavy precipitation has been clearly documented (Maddox et al. 1979, 1980; Funk 1991). The inclusion of cold pools in the initial conditions of operational models should assist forecasters in focusing upon the most likely regions for the development of severe weather and heavy precipitation.

Unfortunately, cold pools are not well sampled by the routine observational systems and thus, in this study, are identified using a very simple procedure based upon a bandpass analysis of the sea level pressure field in conjunction with the multisensor national precipitation analysis. Once identified, a conceptual model of the cold pool vertical structure is used to insert the cold pool into the model initial conditions. Other approaches, such as assimilation of precipitation data (Lin et al. 1997), and better use of the WSR-88D, satellite, and radar wind profiler data within the approach documented in this study, should be explored, as these may lead to the improved initialization of cold pool structures. The difficulty with any four-dimensional data assimilation approach is that it depends heavily upon the physical parameterization schemes within the numerical model to create the correct cold pool structures. The current version of the Eta Model uses the Betts–Miller–Janjic convective scheme, which does not include the effects of downdrafts and is not able to create cold pools. Experiences with other mesoscale models suggests that microphysical parameterization schemes with at least four precipitation type categories (cloud water, rain, snow, ice) are needed to produce strong cold pools (Zhang and Gao 1989). Thus, modifications to both the convective and microphysical schemes are necessary before this type of data assimilation approach would be feasible in the present operational model suite.

Regardless of what approaches are used to implement such a cold pool initialization, the results presented here indicate that the incorporation of mesoscale features into operational model initial conditions is an important concern and should be explored further. The lack of mesoscale data spacing for upper-air observations suggests that new and innovative strategies must be developed that make the best use of the available observational data.

Acknowledgments. This work was supported in part by a National Oceanic and Atmospheric Administration–United States Weather Research Program grant during 1996. Danny Mitchell and Mike Baldwin assisted in accessing the precipitation datasets and their help is greatly appreciated. Reviews of the manuscript by John Kain, Ed Szoke, Keith Brewster, and one anonymous reviewer helped to clarify our presentation and are greatly appreciated.

REFERENCES

Baldwin, M. E., and K. E. Mitchell, 1996: The NCEP hourly multisensor U.S. precipitation analysis. Preprints, *11th Conf. on Numerical Wea. Prediction,* Norfolk, VA, Amer. Meteor. Soc., J95–J96.

Barnes, S. L., 1964: A technique for maximizing details in numerical weather maps. *J. Appl. Meteor.,* **3,** 396–409.

——, 1973: Mesoscale objective map analysis using weighted time series observations. NOAA Tech. Memo. ERL NSSL-62, 60 pp. [NTIS COM-73-10781.]

Betts, A. K., 1986: A new convective adjustment scheme. Part I: Observational and theoretical basis. *Quart. J. Roy. Meteor. Soc.,* **112,** 677–691.

——, and M. J. Miller, 1986: A new convective adjustment scheme. Part II: Single column tests using GATE wave, BOMEX, and arctic air-mass data sets. *Quart. J. Roy. Meteor. Soc.,* **112,** 693–709

Black, T. L., 1994: The new NMC mesoscale eta model: Description and forecast experiments. *Wea. Forecasting,* **2,** 266–278.

Blumen, W., 1972: Geostrophic adjustment. *Rev. Geophys. Space Phys.,* **10,** 485–528.

Byers, H. R., and R. R. Braham Jr., 1949: *The Thunderstorm.* U.S. Government Printing Office, 287 pp.

Charba, J. P., and W. H. Klein, 1980: Skill in precipitation forecasting in the National Weather Service. *Bull. Amer. Meteor. Soc.,* **61,** 1546–1555.

Chen, F., and Coauthors, 1996: Modeling of land-surface evaporation by four schemes and comparisons with FIFE observations. *J. Geophys. Res.,* **101,** 7251–7268.

Cortinas, J. V., Jr., and D. J. Stensrud, 1995: The importance of understanding mesoscale model parameterization schemes for weather forecasting. *Wea. Forecasting,* **10,** 716–740.

Davies-Jones, R. P., D. Burgess, and M. Foster, 1990: Test of helicity as a tornado forecast parameter. Preprints, *16th Conf. Severe Local Storms,* Kananaskis Park, AB, Canada, Amer. Meteor. Soc., 588–592.

DiMego, G. J., 1988: The National Meteorological Center Regional Analysis System. *Mon. Wea. Rev.,* **116,** 977–1000.

Doswell, C. A., III, 1977: Obtaining meteorologically significant surface divergence fields through the filtering property of objective analysis. *Mon. Wea. Rev.,* **105,** 885–892.

——, 1987: The distinction between large-scale and mesoscale contribution to severe convection: A case study. *Wea. Forecasting,* **2,** 3–16.

——, S. J. Weiss, and R. H. Johns, 1993: Tornado forecasting—A review. *Proceedings of Tornado Symposium, III, Geophys. Monogr.,* No. 79, Amer. Geophys. Union, 557–571.

Fritsch, J. M., J. Kapolka, and P. A. Hirschberg, 1992: The effects of sub-cloud-layer diabatic processes on cold air damming. *J. Atmos. Sci.,* **49,** 49–70.

Fujita, T., 1959: Study of mesosystems associated with stationary radar echoes. *J. Meteor.,* **16,** 38–52.

Funk, T. W., 1991: Forecasting techniques utilized by the Forecast Branch of the National Meteorological Center during a major convective rainfall event. *Wea. Forecasting,* **6,** 548–564.

Gallus, W. A., Jr., and J. F. Bresch, 1997: An intense small-scale wintertime vortex in the midwest United States. *Mon. Wea. Rev.,* **125,** 2787–2807.

Gutman, G., and A. Ignatov, 1998: The derivation of the green vegetation fraction from NOAA/AVHRR for use in numerical weather prediction models. *Int. J. Remote Sens.,* **19,** 1533–1543.

Heideman, K. F., and J. M. Fritsch, 1988: Forcing mechanisms and other characteristics of significant summertime precipitation. *Wea. Forecasting,* **3,** 115–130.

Janjic, Z. I., 1994: The step-mountain eta coordinate model: Further developments of the convection, viscous sublayer, and turbulence closure schemes. *Mon. Wea. Rev.,* **122,** 927–945.

Johns, R. H., and C. A. Doswell III, 1992: Severe local storms forecasting. *Wea. Forecasting,* **7,** 588–612.

Unauthenticated | Downloaded 05/11/21 01:50 AM UTC

Kain, J. S., M. E. Baldwin, D. J. Stensrud, T. L. Black, and G. S. Manikin, 1998: Considerations for the implementation of a convective parameterization scheme in an operational mesoscale model. Preprints, *12th Conf. on Numerical Weather Prediction,* Phoenix, AZ, Amer. Meteor. Soc., 103–106.

Lin, Y., K. Mitchell, E. Rogers, and M. Baldwin, 1997: Assimilation of real-time, multi-sensor hourly precipitation observations into the NCEP Eta Model. Preprints, *12th Conf. on Numerical Weather Prediction,* Phoenix, AZ, Amer. Meteor. Soc., 174–175.

Maddox, R. A., 1980: An objective technique for separating macroscale and mesoscale features in meteorological data. *Mon. Wea. Rev.,* **108,** 1108–1121.

——, C. F. Chappell, and L. R. Hoxit, 1979: Synoptic and meso-α scale aspects of flash flood events. *Bull. Amer. Meteor. Soc.,* **60,** 115–123.

——, L. R. Hoxit, and C. F. Chappell, 1980: A study of tornadic thunderstorm interactions with thermal boundaries. *Mon. Wea. Rev.,* **108,** 322–336.

Mellor, G. L., and T. Yamada, 1982: Development of turbulence closure model for geophysical fluid problems. *Rev. Geophys. Space Phys.,* **20,** 851–875.

Mesinger, F., Z. I. Janjic, S. Nickovic, D. Gavrilov, and D. G. Deaven, 1988: The step-mountain coordinate: Model description and performance for cases of Alpine lee cyclogenesis and for a case of Appalachian redevelopment. *Mon. Wea. Rev.,* **116,** 1493–1518.

Mostek, A. J., and N. W. Junker, 1989: Quantitative precipitation forecast verification at the National Meteorological Center. Preprints, *12th Conf. on Weather Analysis and Forecasting,* Monterey, CA, Amer. Meteor. Soc., 633–639.

Olson, D. A., 1985: The impact of existing boundaries on the usefulness of operational model QPF. Preprints, *Sixth Conf. on Hydrometeorology,* Indianapolis, IN, Amer. Meteor. Soc., 277–283.

Pan, H.-L., and L. Mahrt, 1987: Interaction between soil hydrology and boundary-layer development. *Bound.-Layer Meteor.,* **38,** 185–202.

Rasmussen, E. N., J. M. Straka, R. Davies-Jones, C. A. Doswell III, F. H. Carr, M. D. Eilts, and D. R. MacGorman, 1994: Verification of the origin of rotation in tornadoes experiment: VORTEX. *Bull. Amer. Meteor. Soc.,* **75,** 995–1006.

Rogers, E., D. G. Deaven, and G. J. DiMego, 1995: The regional analysis system for the operational eta model: Original 80 km configuration and recent changes. *Wea. Forecasting,* **10,** 810–825.

——, T. L. Black, D. G. Deaven, G. J. DiMego, Q. Zhou, M. Baldwin, N. W. Junker, and Y. Lin, 1996: Changes to the operational ''early'' eta analysis/forecast system at the National Centers for Environmental Prediction. *Wea. Forecasting,* **11,** 391–413.

Schmidt, J. M., and W. R. Cotton, 1989: A high plains squall line associated with severe surface winds. *J. Atmos. Sci.,* **46,** 281–302.

Spencer, P. L., and D. J. Stensrud, 1998: Simulating flash flood events: Importance of the subgrid representation of convection. *Mon. Wea. Rev.,* **126,** 2884–2912.

Stensrud, D. J., and R. A. Maddox, 1988: Opposing mesoscale circulations: A case study. *Wea. Forecasting,* **3,** 189–204.

——, and J. M. Fritsch, 1994a: Mesoscale convective systems in weakly forced large-scale environments. Part II: Generation of a mesoscale initial condition. *Mon. Wea. Rev.,* **122,** 2068–2083.

——, and ——, 1994b: Mesoscale convective systems in weakly forced large-scale environments. Part III: Numerical simulations and implications for operational forecasting. *Mon. Wea. Rev.,* **122,** 2084–2104.

Wakimoto, R. M., 1982: The life cycle of thunderstorm gust fronts as viewed with Doppler radar and rawinsonde data. *Mon. Wea. Rev.,* **110,** 1060–1082.

Wilks, D. S., 1995: *Statistical Methods in the Atmospheric Sciences: An Introduction.* Academic Press, 467 pp.

Wilson, J. W., and W. E. Schreiber, 1986: Initiation of convective storms at radar-observed boundary-layer convergence lines. *Mon. Wea. Rev.,* **114,** 2516–2536.

Young, G., and J. M. Fritsch, 1989: A proposal for general conventions in analysis of mesoscale boundaries. *Bull. Amer. Meteor. Soc.,* **70,** 1412–1421.

Zhang, D.-L., and K. Gao, 1989: Numerical simulation of an intense squall line during 10–11 June 1985 PRE-STORM. Part II: Rear inflow, surface pressure perturbations and stratiform precipitation. *Mon. Wea. Rev.,* **117,** 2067–2094.

Zhao, Q., T. L. Black, and M. Baldwin, 1997: Implementation of the cloud scheme in the Eta Model at NCEP. *Wea. Forecasting,* **12,** 697–712.

Unauthenticated | Downloaded 05/11/21 01:50 AM UTC